Article

Cell Stem Cell

Chromatin Accessibility Dynamics during Chemical Induction of Pluripotency

Graphical Abstract

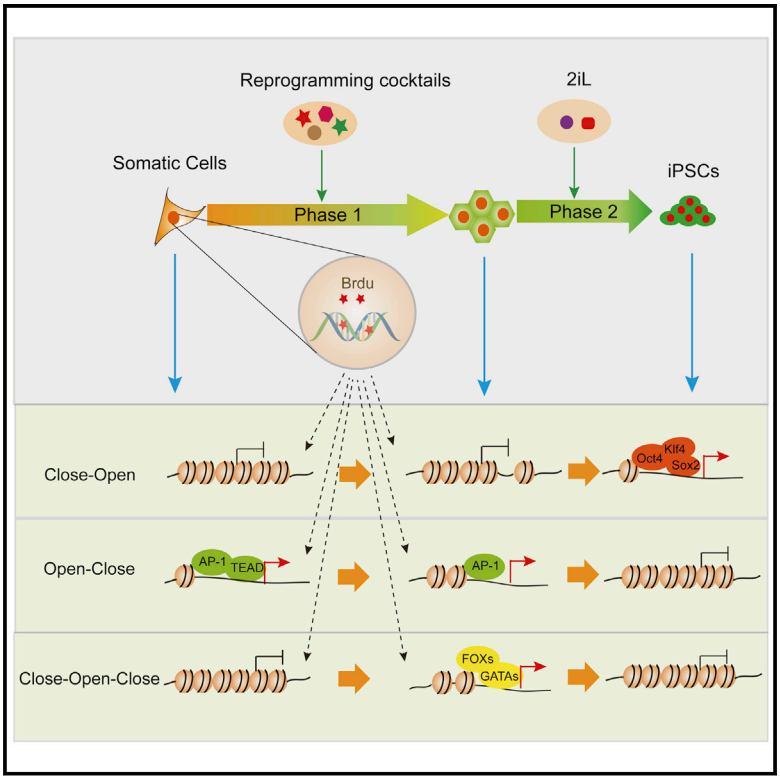

Authors

Shangtao Cao, Shengyong Yu, Dongwei Li, ..., Jiekai Chen, Jing Liu, Duanqing Pei

Correspondence

liu_jing@gibh.ac.cn (J.L.), pei_duanqing@gibh.ac.cn (D.P.)

In Brief

Cao et al. report an efficient protocol for chemical induction of pluripotency and its chromatin accessibility dynamics, which links small molecules and the reorganization of nuclear architecture in the context of cell-fate decisions.

Highlights

- CIP occurs in two stages mediated by serum-free chemical cocktail and 2iL
- ATAC-seq-based chromatin accessibility dynamics in CIP differ from OSK reprogramming
- CAD highlight the role of GATAs, SOXs, and FOXs during CIP
- CADs with or without BrdU reveal a key role in reorganizing chromatin

Cao et al., 2018, Cell Stem Cell *22*, 529–542
April 5, 2018
https://doi.org/10.1016/j.stem.2018.03.005

CellPress

Cell Stem Cell
Article

Chromatin Accessibility Dynamics during Chemical Induction of Pluripotency

Shangtao Cao,[1,2,4,8] Shengyong Yu,[1,2,8] Dongwei Li,[1,2,8] Jing Ye,[1,2] Xuejie Yang,[1,2,4] Chen Li,[1,2,4] Xiaoshan Wang,[1,2,3,4] Yuanbang Mai,[1,2] Yue Qin,[1,2,4] Jian Wu,[1,2,4] Jiangping He,[1,2,4] Chunhua Zhou,[1,2,4] He Liu,[1,2,4] Bentian Zhao,[1,2] Xiaodong Shu,[1,2,3] Chuman Wu,[1,2] Ruiping Chen,[5] Waiyee Chan,[6] Guangjin Pan,[1,2,3] Jiekai Chen,[1,2,3,6,7] Jing Liu,[1,2,6,7,*] and Duanqing Pei[1,2,3,6,7,9,*]

[1]CAS Key Laboratory of Regenerative Biology, South China Institute for Stem Cell Biology and Regenerative Medicine, Guangzhou Institutes of Biomedicine and Health, Chinese Academy of Sciences, Guangzhou 510530, China
[2]Guangdong Provincial Key Laboratory of Stem Cell and Regenerative Medicine, South China Institute for Stem Cell Biology and Regenerative Medicine, Guangzhou Institutes of Biomedicine and Health, Chinese Academy of Sciences, Guangzhou 510530, China
[3]Guangzhou Branch of the Supercomputing Center of Chinese Academy of Sciences, Guangzhou 510530, China
[4]University of Chinese Academy of Sciences, Beijing 100049, China
[5]School of Medicine, South China University of Technology, Guangzhou 510006, China
[6]CUHK-GIBH Joint Laboratory of Stem Cell and Regenerative Medicine, Chinese University of Hong Kong, Shatin, Hong Kong SAR, China
[7]GUANGZHOU Regenerative Medicine and Health Guangdong Laboratory at GIBH, Guangzhou 510530, China
[8]These authors contributed equally
[9]Lead Contact
*Correspondence: liu_jing@gibh.ac.cn (J.L.), pei_duanqing@gibh.ac.cn (D.P.)
https://doi.org/10.1016/j.stem.2018.03.005

SUMMARY

Despite its exciting potential, chemical induction of pluripotency (CIP) efficiency remains low and the mechanisms are poorly understood. We report the development of an efficient two-step serum- and replating-free CIP protocol and the associated chromatin accessibility dynamics (CAD) by assay for transposase-accessible chromatin (ATAC)-seq. CIP reorganizes the somatic genome to an intermediate state that is resolved under 2iL condition by reclosing previously opened loci prior to pluripotency acquisition with gradual opening of loci enriched with motifs for the OCT/SOX/KLF families. Bromodeoxyuridine, a critical ingredient of CIP, is responsible for both closing and opening critical loci, at least in part by preventing the opening of loci enriched with motifs for the AP1 family and facilitating the opening of loci enriched with SOX/KLF/GATA motifs. These changes differ markedly from CAD observed during Yamanaka-factor-driven reprogramming. Our study provides insights into small-molecule-based reprogramming mechanisms and reorganization of nuclear architecture associated with cell-fate decisions.

INTRODUCTION

The induction of pluripotent stem cells (iPSCs) from somatic cells is a revolutionary concept for biology and medicine (Takahashi et al., 2007; Wu and Hochedlinger, 2011). In particular, the iPSC system offers a unique opportunity to understand the role of transcription factors in determining cell fate alone or in concert (Buganim et al., 2013; Li et al., 2010; Papp and Plath, 2013; Polo et al., 2012; Theunissen and Jaenisch, 2014). The cooperation among the Yamanaka factors orchestrates the reprogramming of cellular and genomic structures necessary for the conversion of somatic cells to pluripotent ones functionally equivalent to embryonic stem cells (ESCs).

It has been proposed that the Yamanaka factors (YFs) may be replaced by chemicals (Pei, 2008, 2009). Indeed, efforts from multiple laboratories have provided evidence that small molecules are capable of replacing YFs (Esteban et al., 2010; Huangfu et al., 2008; Liu et al., 2016; Shi et al., 2008a, 2008b; Xu et al., 2008). For example, vitamin C enhances iPSC generation from both human and mouse cells by functionally replacing Myc (Esteban et al., 2010). RepSox can be used to replace Sox2 (Ichida et al., 2009). BMP4 can be used to replace KLF4 for the epithelialization of the MEFs during MET (Chen et al., 2011b). Armed in part by this knowledge, we and others have been able to generate iPSCs with Oct4 alone with the help of chemical cocktails (Chen et al., 2011b; Li et al., 2011; Zhu et al., 2010). Remarkably, Deng and colleagues reported the replacement of Oct4 with small-molecule Forskolin and developed the first protocol for chemical-induced pluripotent stem cell (CiPSC) generation (Hou et al., 2013). However, the process remains inefficient and lengthy and requires replating cells, even with improvements (Zhao et al., 2015). Interestingly, Xie and colleagues reported that the induction process can be improved further with bromodeoxyuridine or BrdU, a compound routinely used in labeling proliferating cells *in vivo* (Long et al., 2015). These studies established the fact that chemicals, both natural and synthetic, can replace Oct4/Sox2/Klf4/Myc (OSKM) to reprogram cell fate.

We understand very little mechanistically how chemicals reprogram cell fate. In this report, we provide global chromatin accessibility landscapes during the chemical induction of pluripotency from mouse embryonic fibroblasts to iPSCs. Our data suggest that chemical induction of pluripotency (CIP) differs from YF-based approach significantly in reorganizing the

genome architecture. This approach has allowed us to understand the contribution of BrdU to CIP.

RESULTS

CIP without Serum and Replating

Current CIP approaches rely on serum and cell replating and thus may complicate data collection and analysis. To see whether we can perform CIP without serum and replating cells, we reviewed protocols published so far (Chen et al., 2011b; Hou et al., 2013; Long et al., 2015; Zhao et al., 2015) and decided to start with iCD1 (Chen et al., 2011a) and reformulated it into serum-free reprogramming medium (SFRM) through a rational testing algorithm. We first added Vc, bone morphogenetic protein (BMP), and RepSox to the chemical cocktail as previously shown to improve reprogramming efficiency (Chen et al., 2011b). Then FSK and DZNep were included in the chemical cocktail, as these two molecules were reported to activate the expression of Oct4 (Hou et al., 2013; Zhao et al., 2015). We then screened for histone deacetylases (HADC) inhibitors and found VPA capable of further enhancing reprogramming as reported previously (Huangfu et al., 2008). As MET is a critical process for somatic cell reprogramming and Doltl1 inhibitors were reported to enhance reprogramming by promoting MET (Onder et al., 2012), we added two such inhibitors, EPZ5676 and SGC0946, to our cocktail. Then, we further screened and identified AM580 that can enhance somatic cell reprogramming significantly as reported previously (Yang et al., 2015). Last, we tested BrdU as reported (Long et al., 2015) and included it in the cocktail as well. We then optimized these components and arrived at one SFRM that includes Vitamin C, BMP4, RepSox, BrdU, VPA, FSK, AM580, EPZ5676, DZNep, and SGC0946 (Figure 1A). This SFRM can convert MEFs into epithelial clusters, indicative of a mesenchymal to epithelial transition or MET process (Figure 1B). These epithelial clusters can give rise to colonies as early as day 8 (Figure 1B). However, these clusters and colonies are not stable in SFRM (data not shown). We hypothesized that they may be reprogrammed further under ESC conditions. Indeed, when we switched the culture condition from SFRM to the well-established 2iL condition (Silva et al., 2008), GFP^+ colonies can emerge without replating. We show that the optimal timing for the switch is at day 22 that can give rise to more than 800 GFP^+ colonies at day 40 from a starting population of 20,000 cells, thus achieving an efficiency of more than 4% (Figures 1C and 1D). By fluorescence-activated cell sorting (FACS) analysis, GFP^+ cells can reach >43% at day 40 (Figure S1A), suggesting an efficient reprogramming process. Consistently, qRT-PCR analysis of critical genes revealed that mesenchymal, epithelial, and pluripotency-associated genes are activated or repressed quite distinctively during the 40 day induction process (Figure S1B).

To further confirm the pluripotency of CiPSCs, we established stable cell lines from these colonies. These CiPSCs maintain GFP expression and ESC morphology throughout passages (Figure S1C). We show by qRT-PCR that the endogenous pluripotency-associated genes such as *Oct4*, *Nanog*, *Sox2*, *Esrrb*, *Rex1*, *Dppa5a*, *Sall4*, and *Cdh1* have been activated in these CiPSC lines to levels similar to those of mouse embryonic stem cells (mESCs) (Figure S1D). Furthermore, whole genome RNA sequencing (RNA-seq) analysis demonstrated that these CiPSC lines have similar transcriptomic profiles as mESCs (Figure S1E). Consistently, the protein levels for pluripotency-associated genes, such as *Sox2*, *Oct4*, *Nanog*, and *Rex1*, can be further confirmed by immunofluorescence (Figure S1F). We then performed bisulfite DNA sequencing analysis and show that the promoters of Oct4 and Nanog have been demethylated in CiPSCs, suggesting a robust epigenetic reprogramming of these critical pluripotent loci (Figure S1G).

To assess the differentiation potential of CiPSCs, we subcutaneously injected them into NOD-SCID mice. They were able to form teratoma and differentiate into all three germ layers (Figure S1H). In addition, CiPSCs could be maintained with normal karyotype during passages (Figure S1I). We also injected CiPSCs into blastocysts from ICR (Institute for Cancer Research) mice and obtained chimeric mice with germline transmission (Figure S1J). These results suggest that CiPSCs are fully pluripotent.

Based on a previous report that CIP appears to go through an XEN-like stage (Zhao et al., 2015), we investigated this possibility and show that D22 cells from our CIP protocol have similar, but not identical, transcriptomic profiles to both eXEN and D28 cells isolated based on the published protocol (Figures S2A–S2C). We further demonstrate that our D22 cells can incorporate into extraembryonic tissues as eXEN (Figures S2D–S2F). Thus, our CIP reprogramming process appears to go through a similar, but not identical XEN stage as previously reported (Zhao et al., 2015).

BrdU Is Essential for CIP

To determine which of these small molecules are critical for CIP, we performed dropout experiments for each chemical compound and show that BrdU or CHIR99021 (CHIR) are absolutely required (Figure 1E). Meanwhile, dropout of other small molecules or growth factors, such as BMP4, FSK, RepSox, AM580, and basic fibroblast growth factor (bFGF), also significantly reduced the numbers of CiPSCs (Figures 1E and S2G). We then focused on the roles of BrdU and CHIR in chemical reprogramming. We measured cell proliferation in the absence or presence of BrdU or CHIR and observed that the withdrawal of CHIR from chemical cocktails significantly impaired cell proliferation (Figure 1F), suggesting that CHIR contributes to reprogramming primarily through cell proliferation. On the other hand, the dropout of BrdU only slightly impairs cell growth in the first 22 days of reprogramming, suggesting that BrdU works through mechanisms independent of proliferation (Figure 1F). So, we further analyzed the functional consequence of BrdU and CHIR dropout at the first 22 days. We show by qRT-PCR analysis that the withdrawal of BrdU or CHIR impairs not only mesenchymal epithelial transition (MET) (Figure S2H), a process essential for reprogramming (Li et al., 2010; Samavarchi-Tehrani et al., 2010), but also the activation of lineage-specific genes (Figure S2H) (Zhao et al., 2015). Consistently, the expression of selected pluripotency-associated genes such as *Oct4*, *Dppa5a*, *Esrrb*, and *Sall4* was severely impaired by the withdrawal of BrdU or CHIR from SFRM (Figure S2H). These results were further validated by time-course RNA-seq analysis (Figure S2I). Therefore, we conclude that both BrdU and CHIR are required for reprogramming, albeit through different mechanisms.

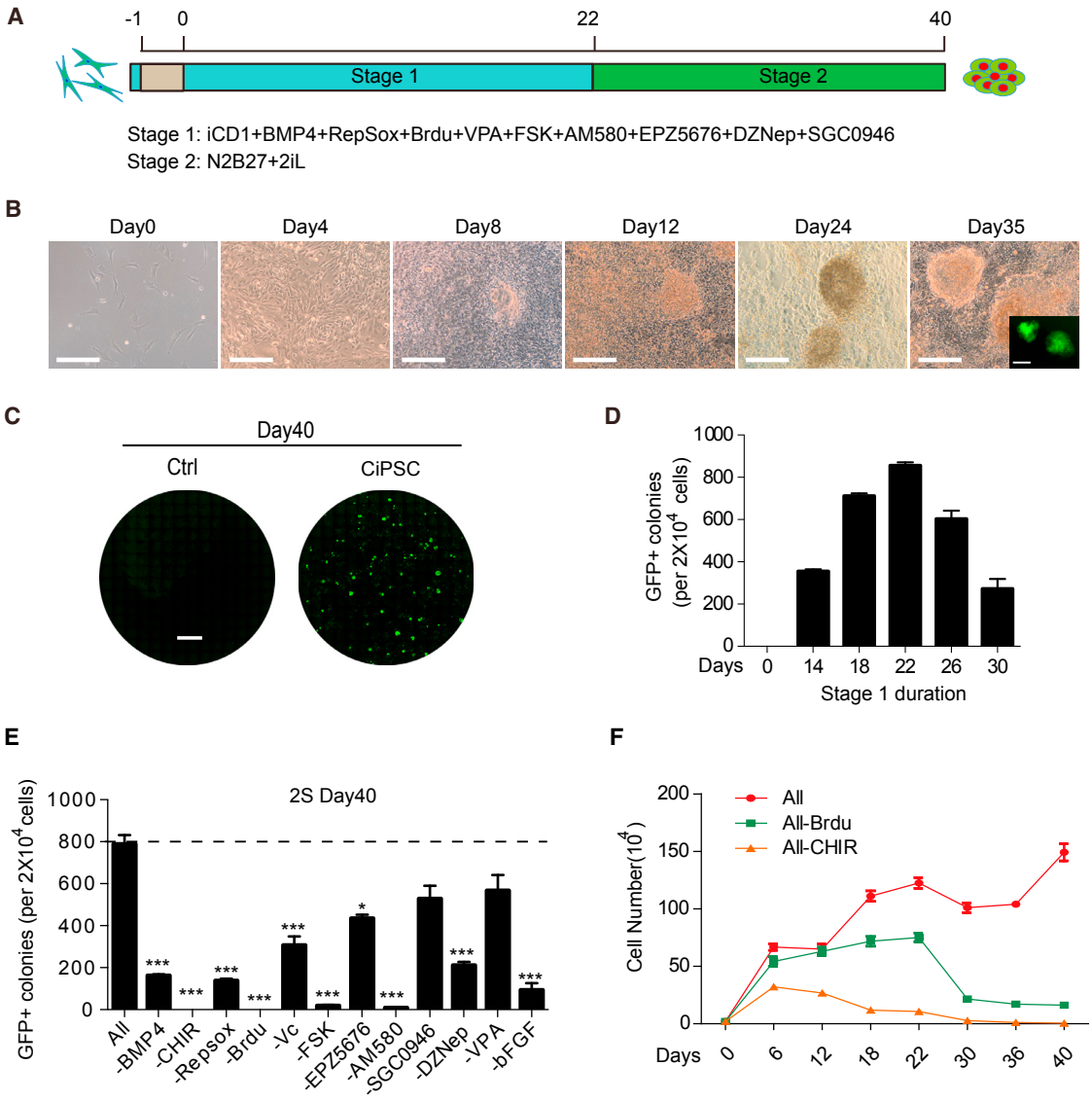

Figure 1. Generation of CiPSCs from MEFs

(A) Schematic diagram for the induction of CiPSCs from MEFs.

(B) Morphological changes at distinct time points during induction of CiPSCs. Scale bars, 250 μm.

(C) Images of GFP$^+$ colonies taken by fluorescence microscope *in situ*. Scale bar, 5 mm.

(D) Numbers of Oct4-GFP+CiPSC colonies generated under indicated conditions. Data are mean ± SD, n = 3 independent experiments.

(E) The effect of individual chemical on the generation of CiPSCs. Data are mean ± SD, n = 3 independent experiments. ***p < 0.001.

(F) The growth curve of cells cultured with or without BrdU or CHIR99021 during CiPSC induction. Data are mean ± SEM, n = 3 independent experiments.

CIP from Other Cell Sources

Since we used MEFs, a mixed-cell population isolated from developing mouse embryos, for our initial optimization process, we needed to confirm that CiPSCs are indeed induced from fibroblast. To this end, we used a FSP1 (Fibroblast Specific Protein1)-tdTomato reporter to track the origin of the CiPSC (Figure S3A). As shown in Figure S3B, the FSP-tdTomato positive MEFs undergo a typical morphology reprogramming as the wild-type MEFs during CIP induction. The isolated tdTomato CiPSCs can be passaged similarly as ESCs morphologically (Figure S3C).

To determine whether other cell types can be reprogramed by CIP, we isolated cells from the three different germ layers including (1) mouse neural stem cells (NSCs); (2) mouse tail tip fibroblast (TTF), mouse neonatal fibroblast (MNF), and mouse lung fibroblast (MLF); and (3) mouse Hepatocytes (Hep) from OG2 transgene mice. All of these cell types can be reprogrammed into typical GFP$^+$ colonies (Figure 2A), albeit with varying degrees of reprogramming efficiency (Figures 2B–2D). We then focused on the MNF-derived CiPSCs for detailed characterizations and show that they can be passaged stably and possessed all the features of pluripotency (Figures 2E–2K)

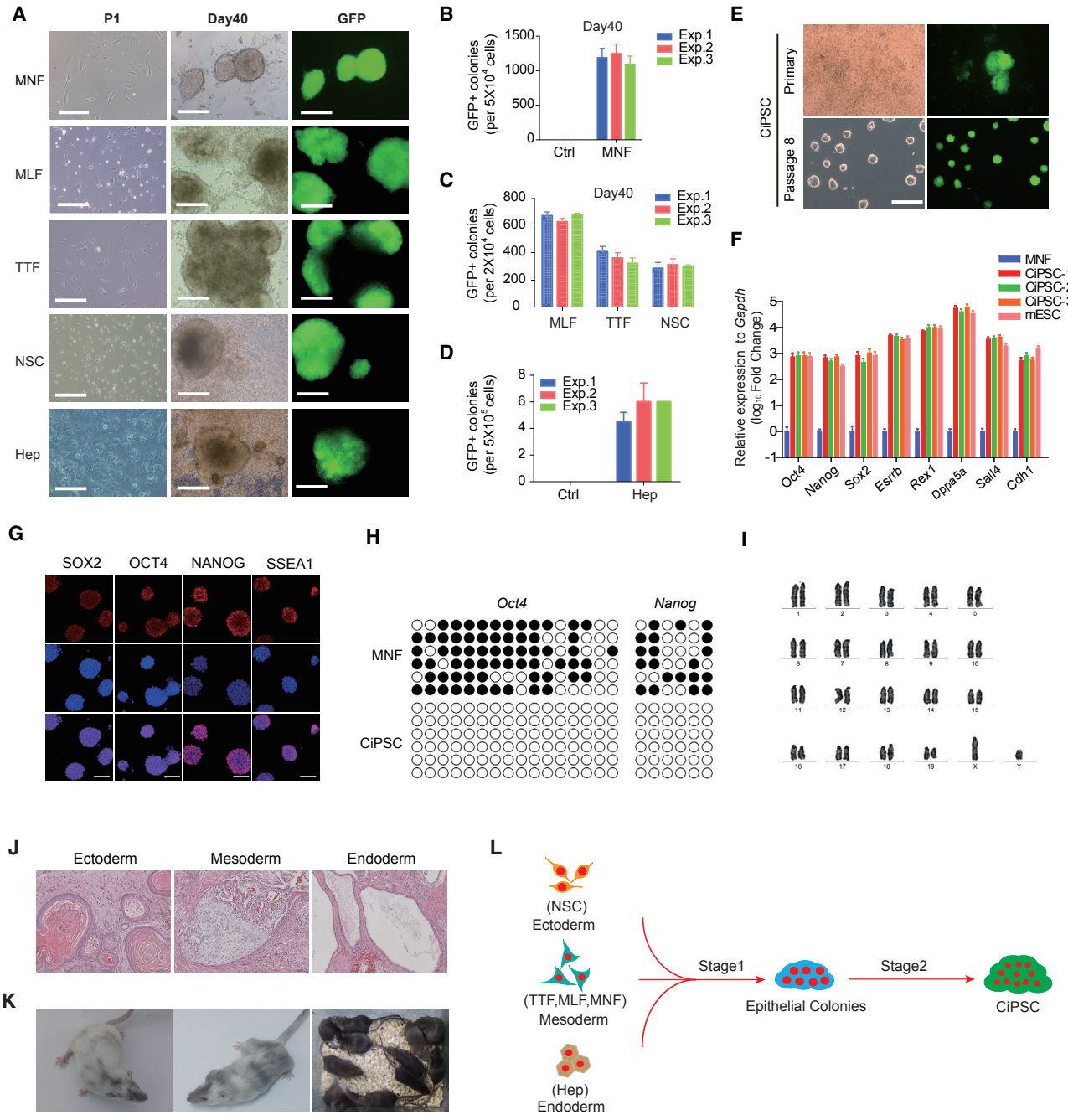

M

	Basic medium	Replate	stages	Time (day)	Efficiency	Reference
Our Lab	Chemical defined	NO	2	35-40	2%-4%	
Deng's	FBS+KSR	Day12 replate	3	40-50	0.2%-0.6% (Replate)	Science, 2013 Cell, 2015 Cell Res, 2016
Xie's	FBS+KSR	Day12 replate	3	55-60	~0.01% (Replate)	Cell Res, 2015

(legend on next page)

including the ability to form chimeric mice with germline transmission.

Taken together, we conclude that the optimized CIP protocol can reprogram somatic cells isolated from different tissues and stages of development into CiPSCs (Figure 2L). Compared to prior protocols (Figure 2M), this protocol is serum free and performed *in situ* without replating can give rise to efficiency on par with YF-based methods. The chemically defined medium used in this protocol has a unique composition compared to the previously published ones (Figure S3D).

CAD during CIP

Genome architecture determines the function state of a cell. The conversion of MEFs into iPSCs by CIP should be one of the ideal systems to probe the reprogramming process at the chromatin level, which may provide a detailed understanding on how chemicals reorganize the overall architecture of a genome from a somatic to a pluripotent state. To answer this question, we performed assay for transposase-accessible chromatin sequencing (ATAC-seq) on MEFs, MEFs undergoing CIP at D6, 12, 18, 22, 30, 36, and finally 40 when CiPSC colonies can be picked up. We first performed a principal-component analysis (PCA) and show that the genome accessibility landscape as assessed by ATAC-seq undergoes gradual transitions that bridge between those of MEFs and ESCs (Figure 3A, left panel, blue arrow). We then compare it with similar dataset obtained from Yamanaka-factor-induced reprogramming (YIP) (Li et al., 2017) and show that CIP and YIP follow quite distinct chromatin accessibility dynamics (CAD) toward pluripotency (Figure 3A, left panel, blue versus red arrows). As chromatin accessibility landscape determines the overall transcription program of a cell, we further compare the transcriptomes between CIP and YIP by PCA analysis and show that CIP and YIP also follow distinct transitions in their transcription programs to arrive at the same pluripotent state (Figure 3A, right panel, blue versus red arrows).

The apparent difference between CIP and YIP further inspired us to investigate in greater detail the CAD for CIP. In our earlier work, we have devised a simple close-open logic for YIP based reprogramming in terms of chromatin accessibility (Li et al., 2017). Accordingly, we first compare the peaks at each locus between MEFs and ESCs and divide the peaks into three categories, closed in MEFs but open in ESCs (CO), open in MEFs but closed in ESCs (OC), open in both MEFs and ESCs (PO). Then the CO and OC peaks of each reprogramming system were further divided into several subgroups based upon the day of reprograming to demonstrate the progression of chromatin accessibility (i.e., opening/closing) dynamics (Figure 3B). Under identical analytic conditions, despite the differences we observe for CIP and YIP in Figure 3A, we arrive at a logic for CIP very similar to that for YIP, i.e., OC at the early stage followed by CO in the late stage (Figure 3B, left versus right panels). In terms of chromatin accessibility landscapes between MEFs and ESCs, CIP closes a great deal of loci that are ultimately closed in ESCs while opens only a small number that are open in ESCs at the first data point D6 (Figure 3B, left panel, OC1 versus CO1, and Figure 3C). In fact, when peaks for all loci are quantified, it is apparent that successful closing of chromatin loci dominates the early part of CIP and this presumably prepares the genome to open the pluripotent loci at the end (Figure 3C). When compared to the same CAD, YIP opens more loci early (Figures 3C versus 3D), perhaps reflecting the fact that O, K, and S can target the pluripotent loci directly. Indeed, when we compare the total CO and OC between CIP and YIP, the Venn diagram showed that CIP shared only 25% (4,265/16,983) in CO peaks, but 80% (34,524/43,049) in OC peaks, and 96% (15,800/16,500) in PO peaks with YIP (Figure 3E). This is quite unexpected as only 4,265 CO loci are shared between CIP and YIP. To further investigate whether the CO/OC or PO peaks are transcriptionally active, we performed H3K27ac chromatin immunoprecipitation sequencing (ChIP-seq) and show that the CO peaks undergo a slow and gradual gain of H3K27ac during reprogramming, in contrast to those OC and PO peaks nicely matched with H3K27ac (Figure 3F). These data indicate that CIP and YIP differ mainly in the opening of pluripotent loci while both close the open chromatin in MEFs (OC) and keep open loci open (PO) in a similar fashion.

CAD and TF Networks

To further understand the transcription factor networks involved in the CADs, we performed motif analysis on the relevant CO, OC, and PO loci discovered by ATAC-seq and identified ~45 DNA binding proteins or transcription factors (Figure 3G). CTCF/BORIS motifs are found in PO and CO loci during CIP as well as YIP (Figure 3G, bottom two rows), indicating that CTCF/BORIS play a general and important role in reprogramming the chromatin accessibility landscapes. GATA1–4 motifs, especially GATA3, are involved in CO1–3 during CIP, but not YIP (Figure 3G, rows 3–6 from bottom). Interestingly, KLF4 and 5 are among CO1–8 in CIP (Figure 3G, rows 7 and 8 from the bottom), indicating a persistent opening of these loci, in a fashion similar to YIP, although the exogenous KLF4 may be responsible

Figure 2. Generation of CiPSCs from Other Cell Types

(A) Represented images of CiPSCs from MNFs, MLFs, TTFs, NSCs, and hepatocytes. Scale bar, 250 μm.

(B–D) Quantification of CIP GFP+ colonies generated by MNF(B), MLF, TTF, and NSC (C), and Hep (D). Data are mean ± SD; n = 3.

(E) Representative fields from the primary CiPSCs (passage 0) at day 40 and the passaged CiPSCs cell lines from MNFs (passage 8). Scale bar, 250 μm.

(F) Expression of pluripotency markers in MNFs, mESCs, and three independent CiPSCs lines derived from MNFs by qRT-PCR. Data are mean ± SD, n = 3 independent experiments.

(G) Expression of Sox2, Oct4, NANOG, and SSEA1 in MNF derived CiPSC colonies as detected by Immunofluorescence. Scale bars, 100 μm.

(H) The methylation patterns for the promoter regions of Oct4 and Nanog in MNFs and CiPSC clones by bisulfite sequencing analysis.

(I) Karyotype analysis of a representative MNF derived CiPSC clone.

(J) H&E staining of teratoma from MNF derived CiPSCs.

(K) Chimeric mice generated from MNF derived CiPSCs and their offsprings.

(L) Schematic diagram for the induction of CiPSCs from cells isolated from three germ layers.

(M) Table presentation of different protocols for CIP.

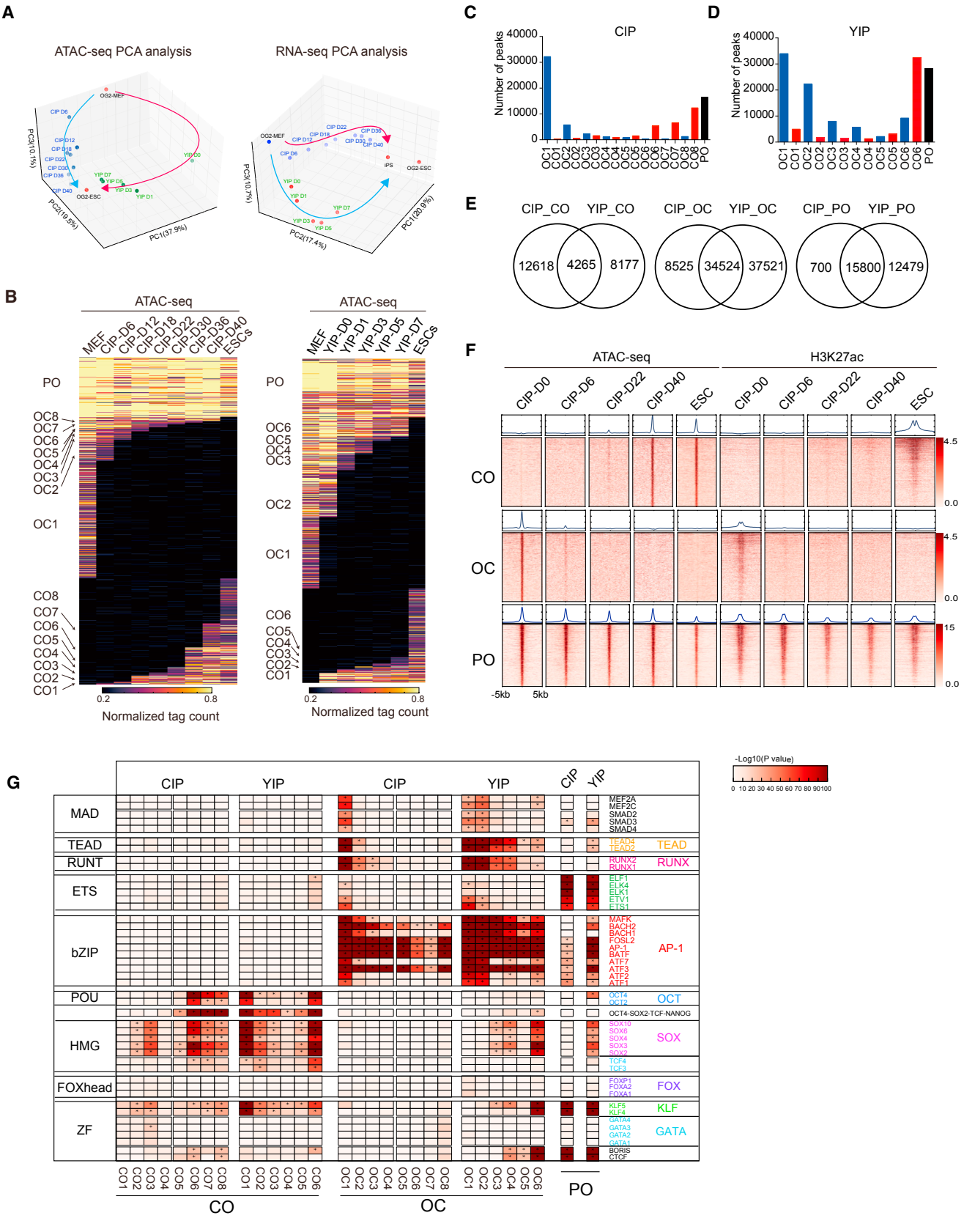

(legend on next page)

for the CO1 in YIP. Like KLF4 and 5, motifs for SOX2–4, 6, and 10 are also found in CO1–8 of CIP, suggesting that CIP preferentially open those loci early (Figure 3G, bottom rows 12–16). Interestingly, motifs for Oct4-Sox2-TCF-Nanog, Oct2, and Oct4 are found in CO5-CO8 of CIP, indicating their opening at very late stage of CIP (Figure 3G, middle rows).

Motifs for the AP1 family of transcription factors (TFs) are very prominent among the OCs during YIP (Li et al., 2017). While ATF1–3 and 7, BATF, AP1, FOSL2, BACH1 and 2, and MAFK are found in OC1 of CIP, many of them persist through OC8 (Figure 3G, middle rows), suggesting that the broad TFs of AP1 family are part of the MEF fate program that must be shut down during reprogramming (Liu et al., 2015). In addition to AP1, motifs for ETS factors are also part of the loci in OC1, RUNX in OC1–3, TEAD in OC1–2, and SMAD2–4/MEF2A/2C in OC1 (Figure 3G, top rows 10–14, 6–9, and 1–5, respectively). Overall, TF motifs for CIP and YIP are quite similar (Figure 3G, OC panel). For the PO loci, both CIP and YIP are quite similar, except the SOX family (Figure 3G, PO panel on the right). Together, we conclude that CIP and YIP reprogram the MEF genome through both common and distinct loci, but clearly through very different dynamics.

Two-Stage Dynamics for CIP

Unlike YIP in which YFs reprogram MEFs to iPSCs in one medium, CIP relies on a two-stage process, first with chemical reprogramming cocktails and second with 2iL (Figure 1A). More critically, we have shown that the first stage is optimal in 22 days and any extension beyond this limit is detrimental to reprogramming (Figure 1D). Therefore, we hypothesize that the first stage plays a critical role in reprogramming as the second stage is under 2iL (Ying et al., 2008). To test this hypothesis, we reanalyzed CIP as two separate stages. When split into two stages but analyzed under the same condition, the CADs of CIP are displayed with greater details (Figures 4A and 4B). Both stages again appear to follow the same close-open logic as shown previously (Li et al., 2017) (Figure 3B) but provide a much clearer stepwise reprogramming process. Using D22 as the reference point, we show that stage 1 of CIP first closes more than 50,000 loci in OC1 and opens >55,000 loci in CO4, suggesting that the opening and closing activities are quite robust at stage 1 (Figure 4C, left panel). On the other hand, using D22 as a starting point, we show that stage 2 starts with the closing of more than 47,000 loci in OC1, and gradually opens loci throughout CO1–4 (Figure 4C, right panel). Consistently, we also find strong correlations between the CO/OC/PO peaks and H3K27ac modification at each stage (Figure 4D). Interestingly, the robust activation of genes in stage 1 suggests that many of those are not for pluripotent loci (Figures 3C versus 4C, left panel). Indeed, only a small fraction of loci for CO1–4 remain open at the pluripotent stage (for example, CO4 in Figure 3C versus CO4 in Figure 4C), thus providing an explanation for the requirement of the lengthy 22 days for stage 1 and also suggesting that many of the CO1–4s undergo a closing process at stage 2. Indeed, 45,318 loci among 72,014 CO loci of stage 1 were closed at stage 2 (Figure S4A, left panel). Specially, 25,574 loci among 47,077 OC1 loci for stage 2 were from CO4 of stage 1 (Figure S4A, right panel). For example, loci near *Sox17* and *Foxa2* are first opened in stage 1 but gradually closed in stage 2 (Figure 4E, left panels). On the other hand, loci near *Sox2*, *Klf2*, and *Dppa2* are opened late at stage 2 (Figure 4E, right panel). To investigate the main biological processes involved in the two individual stages of CIP, we analyzed the gene expression changes coupled with the CADs in each stage. In stage 1, Gene Ontology (GO) analysis reveals that the upregulated genes near CO1–4 peaks are involved in the regulation of phosphoprotein, transcription, cell differentiation, and cell cycle (Figure S4B, left panel, CO1–4), while the downregulated genes around OC1–4 peaks are for cell adhesion and cell migration (Figure S4B, right panel, OC1–4). In stage 2, the upregulated genes near CO1–3 peaks are involved in neural tube closure, metabolic pathway, stem cell population maintenance, and transcription (Figure S4D, left panel, CO1–3), while the downregulated ones near OC1–3 peaks are for cell proliferation, gene expression, multicellular organism development, peptidyl-tyrosine, and dephosphorylation (Figure S4D, right panel, CO1–3). These analyses provide a comprehensive view of the reprogramming roadmap with both gene expression pattern and CADs during CIP (Figures 4A, 4B, S4B, and S4D). The roadmap includes critical genes such as *Jarid2*, *Tbx3*, *Axin2*, *Lin28a*, *Sall4*, opened in CO1–4 of stage 1 (Figures 4A and S4C), and *Zscan4f*, *Trh*, *Nanog*, *Dppa3*, *Nr5a2*, and *Dppa4* in CO1–3 of stage 2 (Figures 4B and S4E).

To further probe the molecular mechanism in both stages, we performed motif analysis. For stage 1, it involves loci with motifs for SOX 2–4, 6, and 10, KLF4 and 5, and GATA1–4 that are gradually opened, peaking at CO3 (Figure 4F, left panel). Interestingly, while loci with those motifs appear to continue to be opened at CO4, loci with AP1 family motifs also start to be opened (Figure 4F, left panel), indicating that further continuation of CO4 would be detrimental to reprogramming. For the closing of chromatin loci, OC1 of stage 1 is very similar to that analyzed as a whole, except loci containing CTCF/BORIS (Figure 4F versus Figure 3G). For stage 2 with 2iL, loci containing motifs for OCT2 and 4, OCT4-SOX2-TCF-NANOG, SOX2–4, 6, and

Figure 3. Chromatin Accessibility Dynamics for CIP

(A) PCA analysis of chemical induced reprogramming (CIP) and Yamanaka-factor (Oct4/Sox2/Klf4 [OKS])-induced reprogramming (YIP) by ATAC-seq data (left panel) and RNA-seq data (right panel). Note the distinct routes for CIP and YIP. CIP from this study and YIP from Li et al. as a control for this study (Li et al., 2017).

(B) Chromatin loci arranged into groups according to time and status being closed or opened as closed to open (CO) or open-to-closed (OC) or permanently open' (PO). Left panel, CIP; right panel, YIP.

(C) The number of peaks defined in CO/OC and PO in (B) for CIP.

(D) The number of peaks defined in CO/OC and PO in (B) for YIP.

(E) Venn diagrams of CO/OC and PO peaks between CIP and YIP.

(F) Heatmap and pileup of ATAC-seq and H3K27ac ChIP-seq signal for CIP-D0, CIP-D6, CIP-D22, CIP-D40, and ESCs. The heatmap and pileups are centered on the ATAC-seq peak (upstream 5 kb and downstream 5 kb of the peaks).

(G) TF motifs significantly enriched at least >2.0-fold for CO/OC/PO categories of ATAC-seq peaks during CIP and YIP. The motifs for TFs are indicated on the right of the heatmap. *$p < 0.01$.

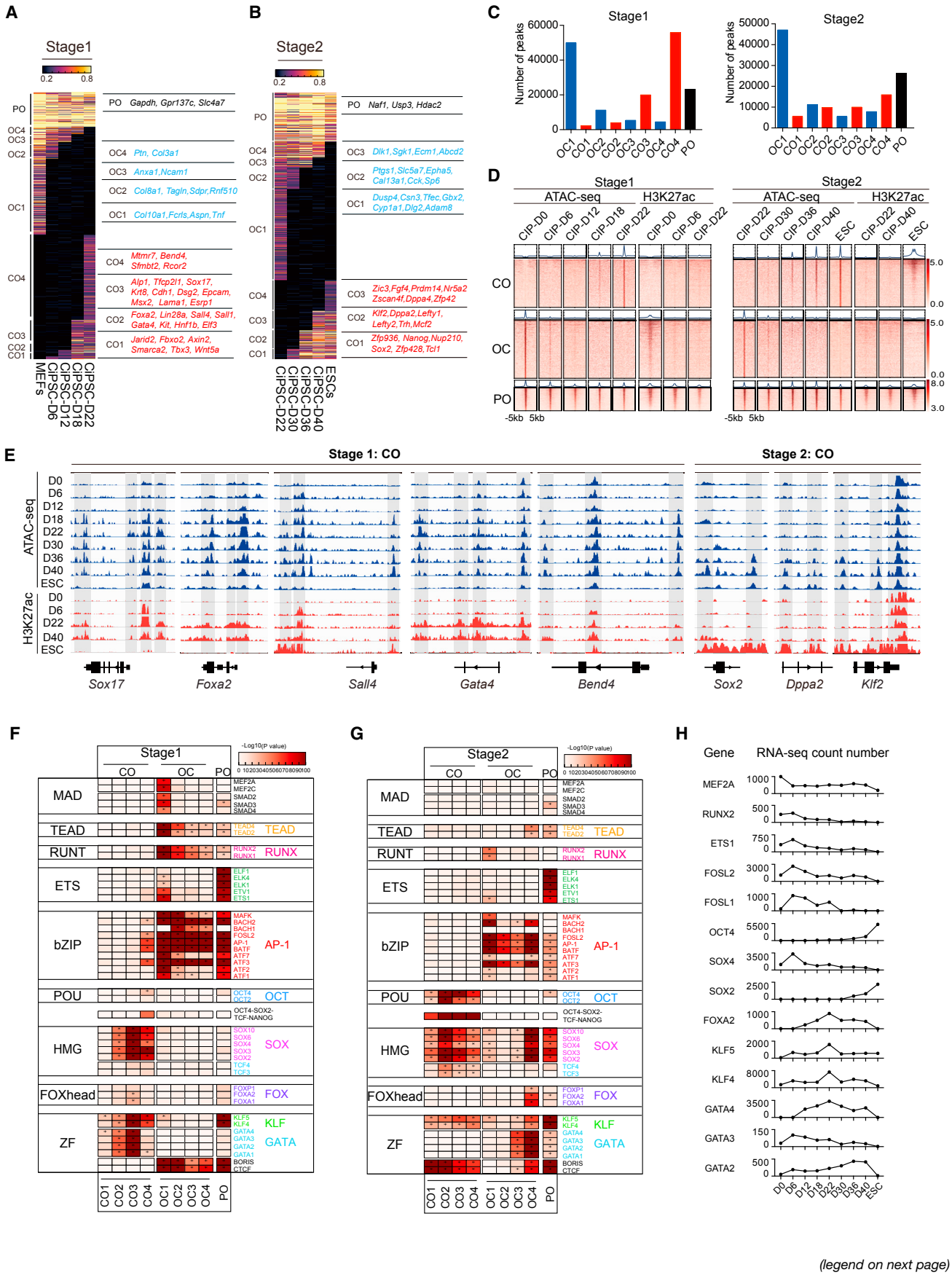

(legend on next page)

10, and KLF4 and 5, along with CTCF/BORIS continue to be opened from CO1–4, while loci with motifs from the AP1, RUNX, ETS, and TEAD closed from OC1–4 (Figure 4G). Interestingly, among the loci that undergo closing are those containing motifs for GATA1–4, KLF4, and 5 and also SOX2–4, 6, and 10 (Figure 4G, right panel), suggesting that many of those opened during stage 1 are undergoing closing before pluripotent network can be established. Consistently, at the transcription level, we observe the induction of GATA2–4, KLF4 and 5, FOXA2, and SOX4 early and their repression late during CIP (Figure 4H), in agreement with the CADs observed, further suggesting that these TFs are activated by CIP to initiate and mediate CAD prior to the establishment of a pluripotent genome architecture.

BrdU Is Required to Open and Close Chromatin

The stepwise CAD of CIP not only provides detailed understanding of chemical reprogramming at the chromatin level but also enables us to ask questions about CIP both mechanistically and practically. To this end, we decide to probe the mechanism through which BrdU facilitates CIP (Figure 1E) (Long et al., 2015). BrdU is a synthetic nucleotide commonly used to label dividing cells by incorporating into newly synthesized DNA (Knobloch et al., 2002; Wojtowicz and Kee, 2006). On the other hand, BrdU has not been associated with cell-fate decision until it was shown to enhance CIP. Interestingly, BrdU has been shown to be able to activate endogenous retrovirus silenced by DNA methylation (Aaronson et al., 1971; Lowy et al., 1971). To probe the role of BrdU in CIP, we cultured cells with or without BrdU for 22 days for the stage 1 of CIP. Without BrdU, MEFs fail to express prominent markers such as *Gata4*, *Sox17*, *Sall4*, instead express *Krt6a*, *Krt5*, and *Kdd2* (Figure 5A), suggesting that MEFs undergoing reprogramming without BrdU have assumed a very different fate. We then mapped CADs during CIP with or without BrdU to show that the CAD is perturbed in such a way that both OC and CO loci failed to be reorganized properly (Figure 5B). We noticed that many loci opened during CIP failed to open without BrdU (Figure 5B, CO1–4 all versus -BrdU). Indeed, when quantified, more than 90% of loci failed to be opened, while ~50% loci closed properly without BrdU (Figure 5C). Consistently, we also find strong correlations between the CO/OC/PO peaks and H3K27ac modification at stage 1 with or without BrdU (Figure 5D). There are significant differences between CO1, CO3, and CO4 and OC1, OC3, and OC4 in loci opening and closing globally with and without BrdU (Figure S5A). For example, *ATF1*, *Bach2*, *Tgfb1i1*, and *Fbln5* loci could not be closed, while loci for *Foxa2*, *Gata4*, *Sall4*, and *Sox17* could not be opened without BrdU (Figure 5E). These results suggest that BrdU can impact the CAD directly.

We further profile the TF motifs associated with CO-OC dynamics and show that loci enriched with motifs for GATA1–4, KLF4 and 5, FOXA1–2, and P1 and SOX2–4, 6, and 10 cannot be opened properly without BrdU (Figure 5F, left panel). On the other hand, the OC and PO loci have very similar TF motif profile with or without BrdU (Figure 5F, right panel). These data suggest that BrdU is responsible for opening up loci enriched for motifs that bind to TFs from GATA, KLF, FOX, and SOX families (Figure 5F). Surprisingly, loci with motifs for the AP1 families of TFs appear to have been opened without BrdU (Figure 5F, left panel on the right side). Consistently, we show that TFs such as GATA4, FOXA2, and SOX17 could not get activated, yet FOSL1 and ATF5 could not be silenced without BrdU at the transcriptional level (Figure 5G), suggesting that BrdU facilitates CIP by both opening and closing chromatin loci critical at stage 1.

We further reasoned that the effect of BrdU should be most profound at the earliest time point. So we decided to analyze both the RNA-seq data and ATAC-seq data with or without BrdU at Day6 in detail. As shown in Figure S5B, the removal of BrdU from CIP results in 1,065 gene upregulated and 1,263 gene downregulated in the RNA-seq dataset, consistent with our earlier analysis that BrdU works by both opening and closing chromatin loci. Indeed, BrdU appears to be responsible for the closing of 4,544 loci and the opening of 3,027 loci (Figure S5C). GO analysis indicates that genes upregulated due to loci opened in a BrdU-dependent manner appear to function in cell adhesion and heart development (Figure S5D, left panel), among which are genes such as *Atp1b1*, *Itgb1*, *Itgb3*, and *Frem2* (Figure S5C), while genes downregulated due to BrdU-dependent closing of loci are enriched with genes such as cytokine-mediated signaling pathway and cell proliferation (Figure S5D, right panel), among which are genes such as *Ccl2*, *Ereg*, and *Sfrp2* (Figure S5C). The functional significance of these genes in reprogramming remains untested. We did test the genes like *Sox17*, *Sall4*, *Gata4*, and *Gate6* activated in a BrdU-dependent manner at stage 1 and show that they could not substitute BrdU (Figure S5E).

BrdU Incorporation Is Required but Not Sufficient to Mediate CIP

BrdU is a thymidine (T) analog known to be able to incorporate into DNA during cell proliferation. As shown in Figure 6A, BrdU can indeed incorporate into cellular DNA during CIP in the first 22 days but gradually be diluted out around day 40. To see whether BrdU mediates CIP in a DNA-incorporation-dependent manner, we synthesized and analyzed more than 20 analogs of BrdU for their ability to incorporate into cellular DNA and induce CiPSCs. We show that 4 analogs, among 11 that can incorporate into DNA (Figures S6A and S6B), can substitute, to some extent,

Figure 4. A Two-Stage CAD for CIP

(A) The global CO/OC and PO status for stage 1 (days 0–22) of CIP (left panel). Representative genes are noted for each subgroup on the right side.

(B) The global CO/OC and PO status for stage 2 (days 22–40) of CIP (left panel). Representative genes are noted in each subgroup at the right.

(C) The number of peaks defined in CO/OC and PO for stage 1 and stage 2 by CIP.

(D) Heatmap and pileup of ATAC-seq and H3K27ac ChIP-seq signals for CIP stage 1 and stage 2, respectively. The heatmap and pileups are centered on the ATAC-seq peak (upstream 5 kb and downstream 5 kb of the peaks).

(E) Representative loci with CO/OC defined by ATAC-seq and corresponding H3K27ac ChIP-seq signals for stage 1 and stage 2, respectively.

(F and G) TF motifs enriched at least 2.0-fold for CO/OC/PO loci defined by ATAC-seq during stage 1 (F) and stage 2 (G) of CIP. TF families are indicated on the right. *$p < 0.01$.

(H) Expression patterns for select genes identified by motif analysis in (F) and (G) by RNA-seq.

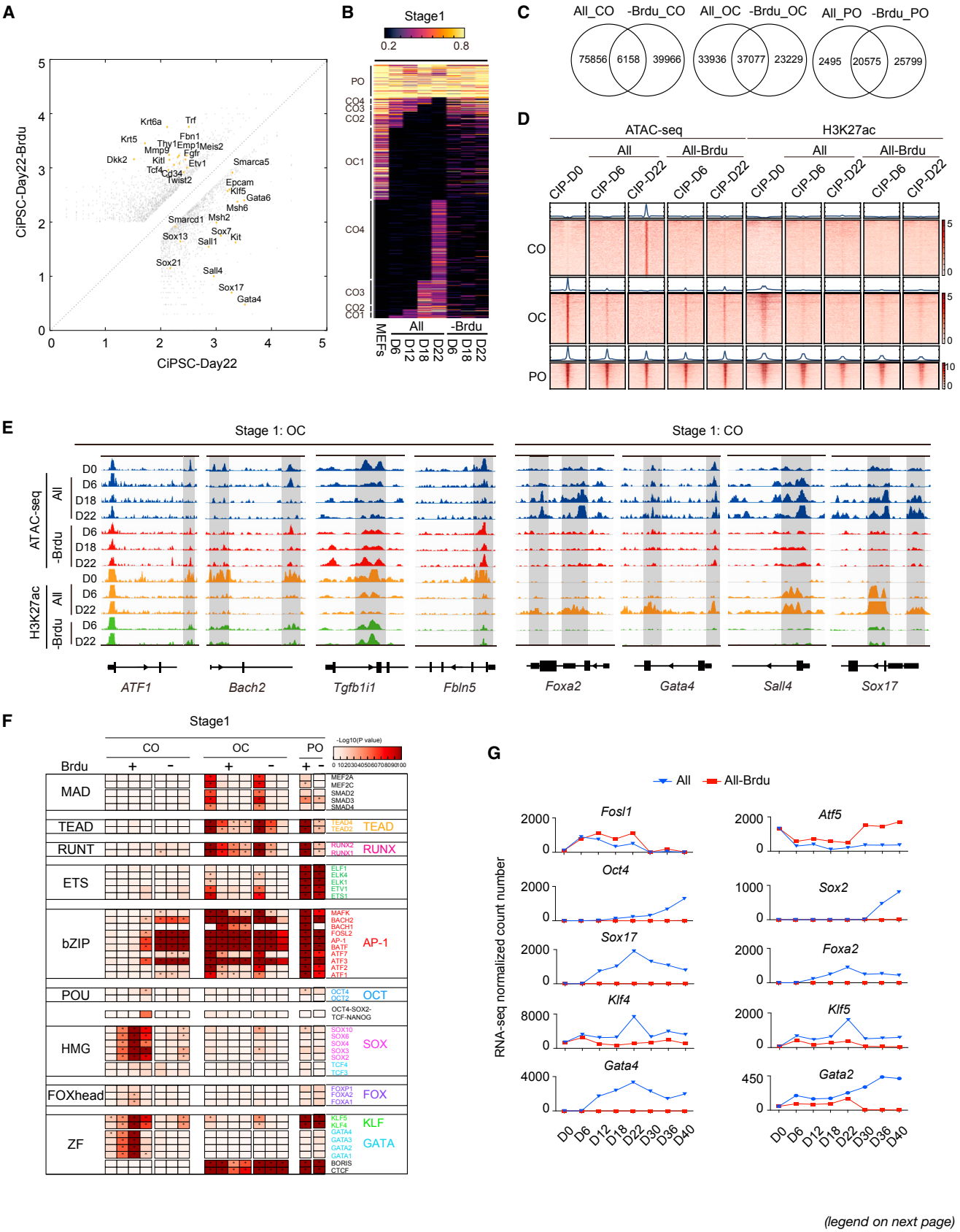

(legend on next page)

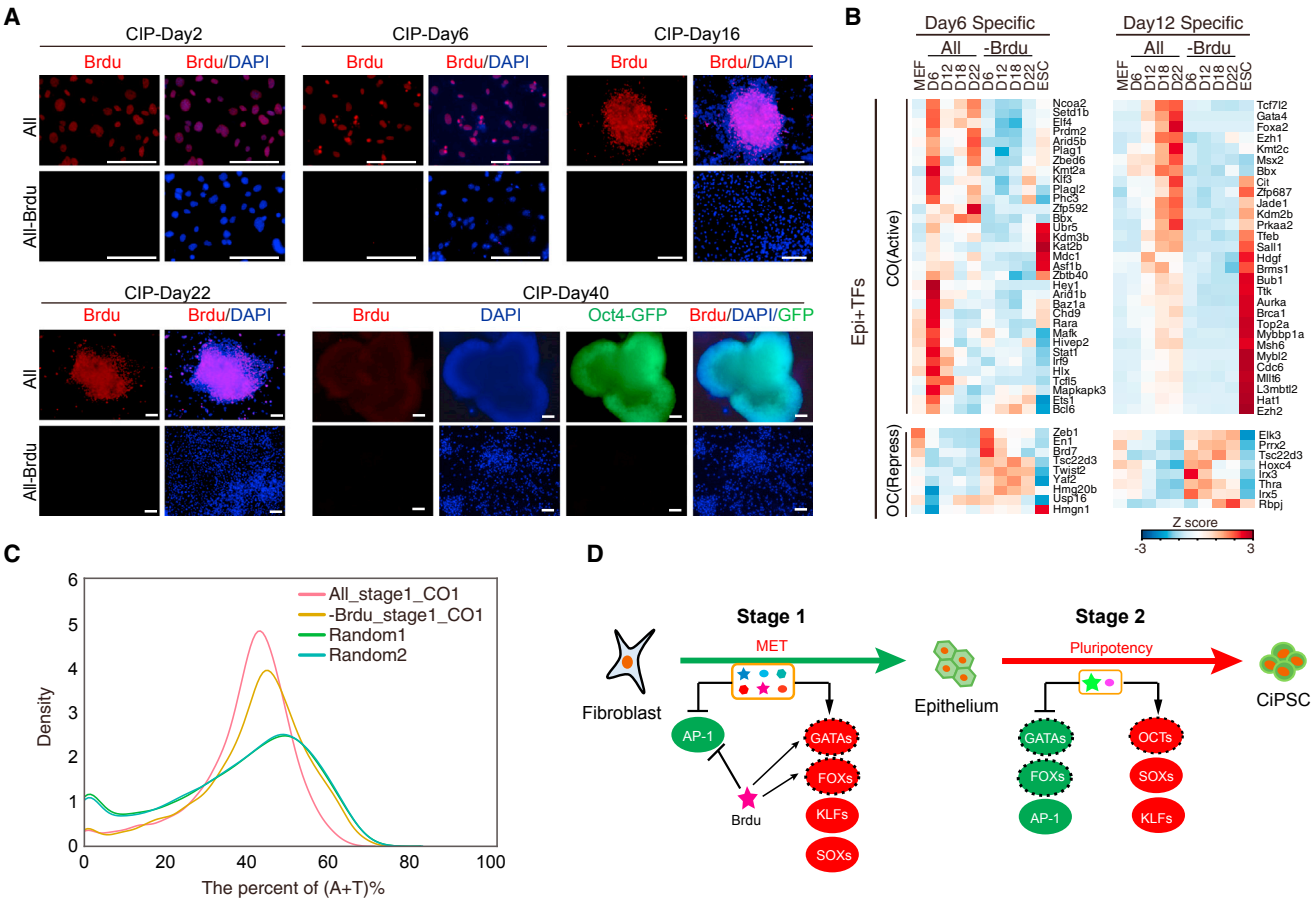

Figure 6. BrdU Modulates Chromatin Structure in CIP

(A) Time-course detection of BrdU incorporation by immunofluorescence. Cells cultured with or without BrdU during CIP at different days were stained with anti-BrdU antibody. Scale bars, 100 μm.

(B) Heatmaps for the expression of nuclear factors in the vicinity of CO/OC peaks with or without BrdU. Nuclear factors upregulated or repressed at day 6 (left) and 12 (right), respectively.

(C) Loci opened in CO1 with or without BrdU as a function of A+T content. Random1/2 are calculated with 10,000 peaks from the ATAC-seq datasets of YIP and CIP. Note the shift of peak to the right without BrdU.

(D) A model for CIP. Stage 1 is accomplished by a cocktail of chemicals and growth factors to close loci enriched with AP1 families of TFs and open those with GATAs, FOXs, KLFs, and SOXs. Stage 2 continues the reprogramming process with 2iL to build the pluripotency network by first closing loci enriched with TFs from GATAs, FOXs, and AP1s, and opening loci with OCTs, SOXs, and KLFs. This model is similar to YIP as MET initiates reprogramming toward building a stable pluripotency network (Li et al., 2010; Polo et al., 2012).

BrdU during CIP (Figure S6C). However, none of the analogs incapable of incorporating into DNA can induce CIP. These results suggest that DNA incorporation is important, but not sufficient for CIP. Consistently, we can detect a gradual induction of epigenetic and TFs in a BrdU-specific manner (Figure 6B). These factors thus constitute a mechanistic apparatus that is responsible for BrdU-mediated CADs during CIP. At the mean time, a relatively small number of TFs and nuclear factors appear to be repressed by BrdU (Figure 6B), consistent with the CO-OC dynamics observed earlier (Figure 3C). Last, we show that BrdU

Figure 5. BrdU Facilitates CIP

(A) Scatterplot showing the difference between transcriptional profiles with or without BrdU at day 22 in CIP.

(B) The global chromatin status of CO /OC and PO arranged as groups during stage 1 of CIP with or without BrdU (days 0–22). Note the failure to open CO1–4 without BrdU on the right.

(C) Venn diagrams of CO/OC and PO peaks between samples with or without BrdU from (B).

(D) Heatmap and pileup of ATAC-seq and H3K27ac ChIP-seq signals for CIP stage 1 with or without BrdU, respectively.

(E) Representative CO/OC peaks from ATAC-seq aligned with H3K27ac ChIP-seq signals for CIP stage 1 with or without BrdU.

(F) TF motifs enriched at least 2.0-fold for CO/OC/PO loci defined by ATAC-seq peaks with or without BrdU at stage 1 of CIP. TF families are indicated on the right of the heatmap. *p < 0.01.

(G) Expression patterns for select genes by RNA-seq.

preferentially impacts DNA loci with relatively low AT content (Figure 6C). Since loci with low AT content are GC rich, thus, more tightly packed than high AT loci at the chromatin level, the incorporation of BrdU in place of T may perturb this tightly packed structure due to its relatively bulky structure (304 dalton) compared to T (~240 dalton). Taken together, these results suggest that BrdU mediates CIP by incorporating into chromatin DNA of reprogramming cells and then reprogramming the CADs physically.

DISCUSSION

CIP holds great promise as a new method to reprogram cell fate. In this report, by removing serum and eliminating replating, we have developed a CIP protocol that allows us to generate iPSCs from MEFs efficiently and perform global mapping of CAD during reprogramming. These datasets should allow detailed comparisons between CIP and the classic Yamanaka approach, i.e., YIP.

One unique feature of our CIP analysis is the two-stage process of induction (Figure 6D). Stage 1 is the most critical one as MEFs are reprogrammed to a state that can be matured into a pluripotent state with 2iL. At stage 1, the reprogramming cocktail closes and opens chromatin loci in MEFs that belong to the AP1 families of TFs and the GATAs, FOXs, KLFs, and SOXs, respectively (Figure 6D). Based on our prior analysis, it is not surprising that the loci closed are enriched with AP1s (Li et al., 2017). It is quite surprising to see FOXs and GATAs in addition to the predicted KLFs and SOXs among the loci opened by the chemical cocktail at stage 1 (Figure 6D). Interestingly, our data indicate that BrdU appears to be responsible for the closing of loci enriched with AP1, and opening of loci enriched with GATAs, FOXs, KLFs, and SOXs (Figure 6D). Thus, these results reveal a causal role of BrdU in closing and opening of chromatin loci, but much work is needed to understand how BrdU can mediate such effects at the molecular level. At the end of stage 1, the cells (D22) appear to assume an XEN-like fate as demonstrated earlier by Deng and colleagues (Zhao et al., 2015), suggesting that CIP goes through an XEN-like intermediate stage. Alternatively, this XEN-like state may be just a parallel fate independent of the the CIP process as reported recently (Parenti et al., 2016). Further work is needed to resolve whether XEN-like states are intermediates or just an alternative fate in parallel.

Stage 2 involves further closing of loci enriched with motifs from TFs of AP1 families, as well as those enriched with GATAs and FOXs opened during stage 1. This is quite different from YIP, which can direct a reprogramming process from MEFs to iPSCs without going through the opening of chromatin loci enriched with GATA and FOX TFs (Figure 4G) (Li et al., 2017). It is quite surprising that such closing is apparently mediated by 2iL. Further studies should be performed to understand the apparent reprogramming power of 2iL.

It would be interesting to understand how 2iL mediates the opening of loci enriched with OCT/SOX/KLF families of TFs (Figure 6D). Apparently, the transition from the intermediate to the pluripotent state is dependent on 2iL. It would be really interesting to identify the mechanism that are responsible for 2iL to mediate the closing and opening of chromatin loci such that a naive genome architecture can be established (Silva et al., 2008).

On a practical note, the CAD defined in this study may help us improve CIP. By comparing the reprogramming processes driven by CIP or the classic YFs, it is clear that the former is too lengthy. It takes about 40 days for quality colonies to emerge from the reprogramming cells versus 7 days for Yamanaka-factor-mediated reprogramming (Chen et al., 2011a). In theory, CIP should be as fast as YIP, i.e., in 7 days or so. One likely solution is to identify unique barriers during CIP through analysis such as CADs and then devise ways to overcome them. To this end, we have made progresses by optimizing CIP under serum-free and non-replating condition. This CIP protocol presented here should be very helpful as a screening platform for these barriers and also facilitators (chemicals both synthetic and natural) that can boost reprogramming chemically. Furthermore, our results on the role of BrdU in CIP suggest that a new class of chemicals that can physically incorporate into DNA can be evaluated for their ability to regulate chromatin dynamics and mediate cell-fate changes both *in vitro* and *in vivo*. Therefore, it is our hope that our work presented here can further inspire effort to improve CIP to a degree on par with the classic Yamanaka approach in both efficacy and timing, and then the CIP platform should become a robust system for cell-fate dissection and also regenerative medicine.

STAR★METHODS

Detailed methods are provided in the online version of this paper and include the following:

- KEY RESOURCES TABLE
- CONTACT FOR REAGENT AND RESOURCE SHARING
- EXPERIMENTAL MODEL AND SUBJECT DETAILS
  - Mice
  - Cell culture
- METHOD DETAILS
  - Culture medium preparation
  - Chemical induction of iPSCs from mouse fibroblasts
  - Chemical induction of iPSCs from mouse primary hepatocytes
  - Chemical induction of iPSCs from mouse neural stem cells
  - Immunofluorescence staining
  - Quantitative RT-PCR and RNA-seq
  - FACS analysis
  - Bisulfite genomic sequencing
  - Teratoma formation and generation of chimeric mouse
  - XEN chimera assay
  - ATAC-seq
  - ATAC-seq bioinformatics analysis and peaks calling
  - Transcription factor motif discovery and gene ontology
- QUANTIFICATION AND STATISTICAL ANALYSIS
- DATA AND SOFTWARE AVAILABILITY

SUPPLEMENTAL INFORMATION

Supplemental Information includes six figures and one table and can be found with this article online at https://doi.org/10.1016/j.stem.2018.03.005.

ACKNOWLEDGMENTS

This work was supported in part by the National Key R&D Program of China (2017YFA0504100, 2016YFA0101800, 2016YFA0100402, and

2016YFA0100801), "Strategic Priority Research Program" of the Chinese Academy of Sciences (XDA16010204), Key Research Program of Frontier Sciences of the Chinese Academy of Sciences (QYZDJ-SSW-SMC009), National Natural Science Foundation of China (31421004, 31530038, 31461143011, 31522033, 31471242, and 31550110206), National Basic Research Program of China (2014CB965200), Science and Technology Planning Project of Guangdong Province (2015B020228003, 2014B050504008, 2014B020225002, 2014B030301058, and 2014B05052012), and International Partnership Program of Chinese Academy of Sciences (154144KYSB20160059). The authors also are grateful for the support from the Guangzhou Branch of the Supercomputing Center of the Chinese Academy of Sciences.

AUTHOR CONTRIBUTIONS

J.L. and S.C. initiated the project and designed the experiments. S.C. performed the reprogramming experiments with S.Y. and C.L. D.L. conducted and performed ATAC-seq experiments with C.W. X.Y. performed the ChIP-seq library construction. J.L., D.L., X.W., Y.M., J.H., and J.W. preformed bioinformatics analysis. J.Y., Y.Q., and C.Z. performed qPCR experiments. H.L. and X.Y. prepared the RNA-seq libraries. B.Z. performed blastocyst injection with R.C. X.S. and J.C. supervised the bioinformatics analysis. W.C. and G.P. supervised the sequencing. J.L. and D.P. supervised the whole study. D.P. supervised the whole study and wrote the manuscript. D.P. conceived the whole study and approved the final version.

DECLARATION OF INTERESTS

The authors declare no competing interests.

Received: October 15, 2017
Revised: February 5, 2018
Accepted: March 9, 2018
Published: April 5, 2018

REFERENCES

Aaronson, S.A., Todaro, G.J., and Scolnick, E.M. (1971). Induction of murine C-type viruses from clonal lines of virus-free BALB-3T3 cells. Science *174*, 157–159.

Buenrostro, J.D., Giresi, P.G., Zaba, L.C., Chang, H.Y., and Greenleaf, W.J. (2013). Transposition of native chromatin for fast and sensitive epigenomic profiling of open chromatin, DNA-binding proteins and nucleosome position. Nat. Methods. *10*, 1213–1218.

Buenrostro, J.D., Wu, B., Chang, H.Y., and Greenleaf, W.J. (2015). ATAC-seq: A Method for Assaying Chromatin Accessibility Genome-Wide. Curr. Protoc. Mol. Biol. *109*, 1–9.

Buganim, Y., Faddah, D.A., and Jaenisch, R. (2013). Mechanisms and models of somatic cell reprogramming. Nat. Rev. Genet. *14*, 427–439.

Chen, J., Liu, J., Chen, Y., Yang, J., Chen, J., Liu, H., Zhao, X., Mo, K., Song, H., Guo, L., et al. (2011a). Rational optimization of reprogramming culture conditions for the generation of induced pluripotent stem cells with ultra-high efficiency and fast kinetics. Cell Res. *21*, 884–894.

Chen, J., Liu, J., Yang, J., Chen, Y., Chen, J., Ni, S., Song, H., Zeng, L., Ding, K., and Pei, D. (2011b). BMPs functionally replace Klf4 and support efficient reprogramming of mouse fibroblasts by Oct4 alone. Cell Res. *21*, 205–212.

Esteban, M.A., Wang, T., Qin, B., Yang, J., Qin, D., Cai, J., Li, W., Weng, Z., Chen, J., Ni, S., et al. (2010). Vitamin C enhances the generation of mouse and human induced pluripotent stem cells. Cell Stem Cell *6*, 71–79.

Heinz, S., Benner, C., Spann, N., Bertolino, E., Lin, Y.C., Laslo, P., Cheng, J.X., Murre, C., Singh, H., and Glass, C.K. (2010). Simple combinations of lineage-determining transcription factors prime cis-regulatory elements required for macrophage and B cell identities. Mol. Cell *38*, 576–589.

Hou, P., Li, Y., Zhang, X., Liu, C., Guan, J., Li, H., Zhao, T., Ye, J., Yang, W., Liu, K., et al. (2013). Pluripotent stem cells induced from mouse somatic cells by small-molecule compounds. Science *341*, 651–654.

Huangfu, D., Maehr, R., Guo, W., Eijkelenboom, A., Snitow, M., Chen, A.E., and Melton, D.A. (2008). Induction of pluripotent stem cells by defined factors is greatly improved by small-molecule compounds. Nat. Biotechnol. *26*, 795–797.

Hutchins, A.P., Jauch, R., Dyla, M., and Miranda-Saavedra, D. (2014). glbase: a framework for combining, analyzing and displaying heterogeneous genomic and high-throughput sequencing data. Cell Regen *3*, 1.

Ichida, J.K., Blanchard, J., Lam, K., Son, E.Y., Chung, J.E., Egli, D., Loh, K.M., Carter, A.C., Di Giorgio, F.P., Koszka, K., et al. (2009). A small-molecule inhibitor of tgf-Beta signaling replaces sox2 in reprogramming by inducing nanog. Cell Stem Cell *5*, 491–503.

Knobloch, J., Kunz, W., and Grevelding, C.G. (2002). Quantification of DNA synthesis in multicellular organisms by a combined DAPI and BrdU technique. Dev. Growth Differ. *44*, 559–563.

Kumar, V., Muratani, M., Rayan, N.A., Kraus, P., Lufkin, T., Ng, H.H., and Prabhakar, S. (2013). Uniform, optimal signal processing of mapped deep-sequencing data. Nat. Biotechnol *31*, 615–622.

Li, R., Liang, J., Ni, S., Zhou, T., Qing, X., Li, H., He, W., Chen, J., Li, F., Zhuang, Q., et al. (2010). A mesenchymal-to-epithelial transition initiates and is required for the nuclear reprogramming of mouse fibroblasts. Cell Stem Cell *7*, 51–63.

Li, Y., Zhang, Q., Yin, X., Yang, W., Du, Y., Hou, P., Ge, J., Liu, C., Zhang, W., Zhang, X., et al. (2011). Generation of iPSCs from mouse fibroblasts with a single gene, Oct4, and small molecules. Cell Res. *21*, 196–204.

Li, D., Liu, J., Yang, X., Zhou, C., Guo, J., Wu, C., Qin, Y., Guo, L., He, J., Yu, S., et al. (2017). Chromatin accessibility dynamics during iPSC reprogramming. Cell Stem Cell *21*, 819–833.

Liu, J., Han, Q., Peng, T., Peng, M., Wei, B., Li, D., Wang, X., Yu, S., Yang, J., Cao, S., et al. (2015). The oncogene c-Jun impedes somatic cell reprogramming. Nat. Cell Biol. *17*, 856–867.

Liu, K., Yu, C., Xie, M., Li, K., and Ding, S. (2016). Chemical modulation of cell fate in stem cell therapeutics and regenerative medicine. Cell Chem. Biol. *23*, 893–916.

Long, Y., Wang, M., Gu, H., and Xie, X. (2015). Bromodeoxyuridine promotes full-chemical induction of mouse pluripotent stem cells. Cell Res. *25*, 1171–1174.

Lowy, D.R., Rowe, W.P., Teich, N., and Hartley, J.W. (1971). Murine leukemia virus: High-frequency activation in vitro by 5-iododeoxyuridine and 5-bromodeoxyuridine. Science *174*, 155–156.

Niakan, K.K., Schrode, N., Cho, L.T., and Hadjantonakis, A.K. (2013). Derivation of extraembryonic endoderm stem (XEN) cells from mouse embryos and embryonic stem cells. Nat. Protoc. *8*, 1028–1041.

Onder, T.T., Kara, N., Cherry, A., Sinha, A.U., Zhu, N., Bernt, K.M., Cahan, P., Marcarci, B.O., Unternaehrer, J., Gupta, P.B., et al. (2012). Chromatin-modifying enzymes as modulators of reprogramming. Nature *483*, 598–602.

Papp, B., and Plath, K. (2013). Epigenetics of reprogramming to induced pluripotency. Cell *152*, 1324–1343.

Parenti, A., Halbisen, M.A., Wang, K., Latham, K., and Ralston, A. (2016). OSKM induce extraembryonic endoderm stem cells in parallel to induced pluripotent stem cells. Stem Cell Reports *6*, 447–455.

Pei, D. (2008). The magic continues for the iPS strategy. Cell Res. *18*, 221–223.

Pei, D. (2009). Regulation of pluripotency and reprogramming by transcription factors. J. Biol. Chem. *284*, 3365–3369.

Polo, J.M., Anderssen, E., Walsh, R.M., Schwarz, B.A., Nefzger, C.M., Lim, S.M., Borkent, M., Apostolou, E., Alaei, S., Cloutier, J., et al. (2012). A molecular roadmap of reprogramming somatic cells into iPS cells. Cell *151*, 1617–1632.

Samavarchi-Tehrani, P., Golipour, A., David, L., Sung, H.K., Beyer, T.A., Datti, A., Woltjen, K., Nagy, A., and Wrana, J.L. (2010). Functional genomics reveals a BMP-driven mesenchymal-to-epithelial transition in the initiation of somatic cell reprogramming. Cell Stem Cell *7*, 64–77.

Shi, Y., Desponts, C., Do, J.T., Hahm, H.S., Schöler, H.R., and Ding, S. (2008a). Induction of pluripotent stem cells from mouse embryonic

fibroblasts by Oct4 and Klf4 with small-molecule compounds. Cell Stem Cell *3*, 568–574.

Shi, Y., Do, J.T., Desponts, C., Hahm, H.S., Schöler, H.R., and Ding, S. (2008b). A combined chemical and genetic approach for the generation of induced pluripotent stem cells. Cell Stem Cell *2*, 525–528.

Silva, J., Barrandon, O., Nichols, J., Kawaguchi, J., Theunissen, T.W., and Smith, A. (2008). Promotion of reprogramming to ground state pluripotency by signal inhibition. PLoS Biol. *6*, e253.

Takahashi, K., Tanabe, K., Ohnuki, M., Narita, M., Ichisaka, T., Tomoda, K., and Yamanaka, S. (2007). Induction of pluripotent stem cells from adult human fibroblasts by defined factors. Cell *131*, 861–872.

Theunissen, T.W., and Jaenisch, R. (2014). Molecular control of induced pluripotency. Cell Stem Cell *14*, 720–734.

Wojtowicz, J.M., and Kee, N. (2006). BrdU assay for neurogenesis in rodents. Nat. Protoc. *1*, 1399–1405.

Wu, S.M., and Hochedlinger, K. (2011). Harnessing the potential of induced pluripotent stem cells for regenerative medicine. Nat. Cell Biol. *13*, 497–505.

Xu, Y., Shi, Y., and Ding, S. (2008). A chemical approach to stem-cell biology and regenerative medicine. Nature *453*, 338–344.

Yang, J., Wang, W., Ooi, J., Campos, L.S., Lu, L., and Liu, P. (2015). Signalling through retinoic acid receptors is required for reprogramming of both mouse embryonic fibroblast cells and epiblast stem cells to induced pluripotent stem cells. Stem Cells *33*, 1390–1404.

Ying, Q.L., Wray, J., Nichols, J., Batlle-Morera, L., Doble, B., Woodgett, J., Cohen, P., and Smith, A. (2008). The ground state of embryonic stem cell self-renewal. Nature *453*, 519–523.

Young, M.D., Wakefield, M.J., Smyth, G.K., and Oshlack, A. (2010). Gene ontology analysis for RNA-seq: accounting for selection bias. Genome Biol. *11*, R14.

Zhao, Y., Zhao, T., Guan, J., Zhang, X., Fu, Y., Ye, J., Zhu, J., Meng, G., Ge, J., Yang, S., et al. (2015). A XEN-like state bridges somatic cells to pluripotency during chemical reprogramming. Cell *163*, 1678–1691.

Zhu, S., Li, W., Zhou, H., Wei, W., Ambasudhan, R., Lin, T., Kim, J., Zhang, K., and Ding, S. (2010). Reprogramming of human primary somatic cells by OCT4 and chemical compounds. Cell Stem Cell *7*, 651–655.

STAR★METHODS

KEY RESOURCES TABLE

REAGENT or RESOURCE	SOURCE	IDENTIFIER
Antibodies		
Mouse monoclonal anti-Oct3/4	Santa Cruz	Cat#sc-5279; RRID: AB_628051
Goat polyclonal anti-Sox2	Santa Cruz	Cat#sc-17320; RRID: AB_2286684
Rabbit polyclonal anti-Nanog	BETHYL	Cat# A300-397A; RRID: AB_386108
Mouse monoclonal anti-SSEA-1	R&D	Cat#MAB2155; RRID: AB_358058
Rabbit polyclonal anti-H3K27ac	Abcam	Cat#ab4729; RRID: AB_2118291
Rabbit polyclonal anti-H3K9me3	Abcam	Cat#ab8898; RRID:AB_306848
Rabbit polyclonal anti-H3K9me3	Abcam	Cat#ab8580; RRID:AB_306649
Mouse anti-Brdu antibody	Sigma	Cat#B2351; RRID:AB_476793
Chemicals, Peptides, and Recombinant Proteins		
Recombinant Human BMP-4	R&D	314-BP;GenPept: Q53XC5
bFGF	PeproTech	GenPept: P09038
Vitamin C	Sigma-Aldrich	49752; CAS: 66170-10-3
Brdu	Sigma-Aldrich	CAS:59-14-3
RepSox	ChemBest	CAS: 446859-33-2
VPA	Sigma-Aldrich	P4543; CAS: 1069-66-5
FSK	ChemBest	CAS:66575-29-9
AM580	Tocris	0760; CAS: 102121-60-8
DZNep	Selleck Chemicals	S7120
EPZ5676	Selleck Chemicals	S7062
SGC0946	Selleck Chemicals	S7079;
EPZ6438	TargetMol	T1788
Capmatinib	TargetMol	T1963
PD0325901	Synthesized in GIBH	N/A
CHIR99021	Synthesized in GIBH	N/A
Leukemia Inhibitory Factor (LIF)	Millipore	Cat#ESGE107
Brdu Analogues1#—24#	Synthesized in GIBH	N/A
Critical Commercial Assays		
SsoAdvanced universal SYBR Green supermix	BIO-RAD	172-5274
Nextera DNA library preparation kit	Illumina	FC-121-1031
KAPA Library Quantification kit	KAPA BIOSYSTEMS	KK4824
TruSeq RNA Sample Prep kit	Illumina	RS-122-2001
VAHTS Turbo DNA Library Prep kit	Vazyme Biotech	TD-503
NextSeq500 High output 150 cycles	Illumina	FC-404-2002
NextSeq500 Mid output 150 cycles	Illumina	FC-404-2001
VAHTSTM Library Quantification Kit	Vazyme Biotech	NQ101-NQ106
AMPure XP beads	BEECKMAN COULTER	A63882
Deposited Data		
RNA-seq data	This paper	GEO: GSE93029 and GEO: GSE110264
ATAC-seq data	This paper	GEO: GSE93029 and GEO: GSE110264
ChIP-seq data	This paper	GEO: GSE110264
Experimental Models: Cell Lines		
OG2-ESCs cell line	This paper	N/A
CiPSCs cell line	This paper	N/A

(*Continued on next page*)

Continued		
REAGENT or RESOURCE	SOURCE	IDENTIFIER
HEK293T	ATCC	CRL-1126
Platinum-E (Plat-E)	A gift from The Fourth Military Medical University	N/A
Mouse primary hepatocytes	This paper	N/A
Mouse primary tail tip fibroblasts	This paper	N/A
Mouse primary lung fibroblasts	This paper	N/A
Mouse neural stem cells	This paper	N/A
Mouse XEN-like cell lines	This paper	N/A
Mouse primary XEN cell lines	This paper	N/A
Experimental Models: Organisms/Strains		
OG2 transgenic mice: CBA/CaJ xC57BL/6J	The Jackson Laboratory	Mouse strain datasheet: 004654
129Sv/Jae mice	Beijing Vital River Laboratory	Mouse strain datasheet: 217
ICR mice	Beijing Vital River Laboratory	Mouse strain datasheet: 201
Oligonucleotides		
Primers for Quantitative RT-PCR	This paper	Table S1
Software and Algorithms		
FlowJo	Ashland	https://www.flowjo.com/solutions/flowjo/downloads
GraphPad Prism 5	GraphPad Software	https://www.graphpad.com/support/faqid/1952/
ZEN 2009	Zeiss	https://www.zeiss.com/microscopy/int/downloads/zen.html
Bio-RAD CFX Manager	BIO-RAD	http://www.bio-rad.com/en-us/product/cfx-manager-software?tab = Download
Accuri C6 Plus	BD biosciences	http://www.bdbiosciences.com/us/instruments/research/cell-analyzers/bd-accuri/m/1294932/overview
Illustrator	Adobe System Software Ireland	https://www.adobe.com/cn/products/cs6/illustrator.html

CONTACT FOR REAGENT AND RESOURCE SHARING

Further information and requests for resources and reagents should be directed to and will be fulfilled by the Lead Contact, Duanqing Pei (pei_duanqing@gibh.ac.cn).

EXPERIMENTAL MODEL AND SUBJECT DETAILS

Mice

Oct4-GFP transgenic allele-carrying mice (CBA/CaJ X C57BL/6J) were from The Jackson Laboratory and 129Sv/Jae and ICR mice were from Beijing Vital River Laboratory. All animal experiments were performed according to the Animal Protection Guidelines of Guangzhou Institutes of Biomedicine and Health, Guangzhou, China.

Cell culture

Mouse embryonic fibroblasts (MEFs) were isolated from E13.5 embryos. In detail, all of the internal organs, head, limbs and tails of the embryos were carefully removed and discarded, the remaining tissues were manually sliced into small pieces and dissociated by the digestive solution (0.25% trypsin: 0.05% trypsin = 1:1; GIBCO) for 15 min at 37°C to obtain a single cell suspension. The cells from each embryo were plated onto one 6-cm 0.1% gelatin coated culture dish in DMEM (Hyclone) supplemented with 10% FBS (GIBCO), 1% GlutaMAX (GIBCO) and 1% NEAA (GIBCO), which was defined as fibroblast medium.

Mouse neonatal fibroblasts (MNFs) were isolated from dorsal skin dermis of day2-3 neonatal pups. Skin tissues were sliced into small pieces about 1 mm^3 and plated onto 6-cm 0.1% gelatin coated culture dishes in fibroblast medium. Generally, fibroblasts move outside from the skin tissues in 2 to 3 days and proliferate up to 90% confluence in 7 to 10 days.

Mouse adult lung fibroblasts (MLFs) and tail tip fibroblasts (TTF) were isolated from 8- week old mice. Mouse adult lung tissues and tails were sliced into small pieces of 1 mm^3 and plated on 6-cm 0.1% gelatin coated culture dishes in fibroblast medium. Generally, fibroblasts move outside from the tissues and grow to 90% confluence in ~10 days.

Mouse neural stem cells (mNSCs) were isolated from the brains of E13.5 embryos under a dissection microscope. Mouse meninges and vessel were removed and discarded. The remaining brain tissues were sliced into small pieces and dissociated by the digestive solution (0.25% trypsin: 0.05% trypsin = 1:1; GIBCO) for 15 min at 37°C and washed with DMEM/12 twice and then plated onto T25 flask bottle in mNSC medium,which is composed of DMEM/F12 (Hyclone) supplemented with 1 x N2 (GIBCO), 1 x B27 (GIBCO), bFGF 20 ng/ml (Peprotech) and EGF 10 ng/ml (Peprotech).

Mouse primary hepatocytes were isolated with the standard two step collagenase perfusion method. Briefly, the mouse liver was pre-perfused through the portal vein with calcium-free buffer (0.5 mM EGTA, Hanks' balanced salt solution without Ca^{2+} and Mg^{2+}) and then perfused with collagenase (0.1 mg/ml collagenase type IV (Sigma), Hanks' balanced salt solution with Ca^{2+} and Mg^{2+}). After perfusion, the livers were excised and pelleted into small pieces in DMEM (Hyclone, high glucose) with an additional 9 mg/ml glucose (Sigma). Then the pellets were washed and centrifuged at low speed (50 g, 5 min) for 2-3 times. The purified primary hepatocytes were stained with 0.04% trypan blue to evaluate the viability, which should exceed 80%, and cultured in HCM medium (Lonza) in Matrigel-coated dishes.

Mouse XEN cells were isolated according to previous studies(Niakan et al., 2013). Briefly, the XEN cells were derived from E3.5 blastocysts and plated on the ICR MEFs feeder in the RPMI1640 (GIBCO) media with 20% FBS, 1% GlutaMAX (GIBCO) and FGF4 20 ng/ml (Peprotech). After 2 weeks, mouse XEN cells move out from the blastocysts and can be used for further passaging.

mESCs and CiPSCs were maintained in feerder free and serum free ESC medium, which is composed of DMEM with N2 (100X), B27 (50X), LIF,1% GlutMax,1%NEAA, beta-mercaptoethanol(0.1 mM), CHIR99021(3 μM) and PD0325901(1 μM).

All the cell lines were mycoplasma free as determined with the Kit from Lonza (LT07-318).

METHOD DETAILS

Detailed protocol for generation of CiPSCs from mouse fibroblasts under chemical defined medium

Culture medium preparation

Stage 1 medium SFRM preparation

iCD1 medium (Chen et al., 2011a) which contains Vitamin C(50 μg/ml), bFGF(10 ng/ml) and CHIR99021(3 μM) supplemented with small molecules Brdu(10 μM), RepSox (5 μM), FSK(10 μM), VPA(0.1 mM), AM580(0.05 μM), EPZ5676(5 μM), DZNeP(0.05 μM), SGC0946(5 μM) and BMP4(10 ng/ml). For the CIP induction from mouse adult lung fibroblasts (MLFs) and tail tip fibroblasts (TTF), 5 μM Capmatinib and 5 μM EPZ6438 were recommended to enhance the induction efficiency.

Stage 2 medium N2B27-2iL preparation

DMEM (high glucose, Hyclone), 1% N2 (GIBCO), 2% B27 (GIBCO), 1% GlutMax (GIBCO), 1% NEAA (GIBCO), 1% sodium pyruvate (GIBCO) 3 μM CHIR99021, 1 μM PD0325901 and 1000 U LIF.

Chemical induction of iPSCs from mouse fibroblasts

The MEFs, MNFs, MLFs and TTFs were seeded at a density of 20,000 cells per well in 12-well plates or 50,000 cells per well in 6-well plates in fibroblast medium, respectively. The culture plates were pre-coated with 0.1% gelatin for more than one hour.

On the next day, the medium was changed into Stage 1 chemical reprogramming medium SFRM (Serum Free Reprograming Medium) and was refreshed every 2 days. The epithelial-like clusters appeared and increased at day 8 and Oct4-GFP positive clusters appeared at day 12. After day 22, the SFRM was replaced with N2B27-2iL medium and was refreshed every 2 days. Oct4-GFP positive ESC-like colonies emerged as early as day 30. During day 36 to 40, Oct4-GFP colonies were counted or detected through FACS.

Note

Because high concentration of DZNep (0.05 μM) or SGC0946 (5 μM) is toxic to the proliferation of mouse adult fibroblasts at stage 1, we used a concentration of 0.01 μM DZNep and 1 μM SGC0946 for the CiPSCs induction from mouse lung fibroblasts and mouse tail tip fibroblasts.

Chemical induction of iPSCs from mouse primary hepatocytes

The mouse primary hepatocytes were seeded at a density of 500,000 to 1,000,000 cells per well in 6-well plates in HCM medium. The culture plates were pre-coated with Matrigel for one hour. After 24 hours, HCM medium was replaced with SFRM medium for 22 days and then changed into N2B27-2iL medium for another 18 days.

Note

We added 5 μM Capmatinib and 5 μM EPZ6438 in SFRM medium to enhance the CIP efficiency.

Because high concentration of DZNep or SGC0946 is toxic to the proliferation of mouse primary hepatocytes at stage 1, we used 0.01 μM DZNep and 1 μM SGC0946 for the CIP of mouse primary hepatocytes.

Because of poor proliferation of mouse primary hepatocytes, a relatively high initial cell density is beneficial to the CIP of mouse primary hepatocytes.

Chemical induction of iPSCs from mouse neural stem cells

The mouse primary neural stem cells were seeded at a density of 20,000 cells per well in 12-well plates in mNSC medium. The culture plates were pre-coated with Matrigel for one hour. After 24 hours, mNSC medium was replaced with SFRM medium for 22 days and then changed into N2B27-2iL medium for another 18 days.

Note

Early passaged cells (from 2 to 5 passage) are ideal to generate CiPSCs from mouse neural stem cells. For late passage ($\geq$10), we recommended 5 μM Capmatinib and 5 μM EPZ6438 in SFRM medium to enhance the CIP efficiency.

Immunofluorescence staining

For immunofluorescence staining, the cells were cultured on coverslips and fixed with 4% paraformaldehyde for 30 min at room temperature. Then, the cells were washed with PBS for three times and permeated with 0.1% Triton X-100 for 30min. Afterward, cells were blocked with 3% BSA in PBS for 1 hour at room temperature and incubated with primary antibodies at 4°C overnight. Then, the cells were washed with PBS for three times and incubated with appropriate secondary antibodies for 1 hour. Further more, the nucleus was counterstained with DAPI. Finally, the coverslips were mounted on the slide for observation under the confocal microscope (Zeiss 710 NLO). Primary and secondary antibodies were diluted in 3% BSA and primary antibodies used in the studies were anti-Oct4 (SC-5279, 1:400), anti-Sox2 (sc-17320, 1:200), anti-Nanog (BETHYL no. A300-397A, 1:200), anti-Rex1 (SC-50668, 1:100) and anti-SSEA1 (RD, MAB2155, 1:100).

Quantitative RT-PCR and RNA-seq

Total RNAs were isolated from cells with TRIzol and converted into cDNAs with ReverTra Ace (Toyobo) and oligo-dT (Takara), and then analyzed by qPCR with Premix Ex Taq (Takara). TruSeq RNA Sample Prep Kit (RS-122-2001, Illumina) was used for library construction and the Miseq Reagent Kit V2 (MS-102-2001, Illumina) was used for RNA-seq.

FACS analysis

The cells were digested by 0.25% trypsin and harvested into tubes and washed with PBS for three times. Then, cells were analyzed by the C6 flow cytometer (Becton Dickinson) and the collected data were analyzed by the software FlowJo7.6.1.

Bisulfite genomic sequencing

Genomic DNA was purified according to manufacturer's protocol (Promega) and was used for bisulfite modification by exposure overnight to a mixture of 50.6% sodium bisulfite and hydroquinone. The promoter regions of Oct4 and Nanog were amplified by PCR. The PCR products were cloned into the pMD18-T vector (Takara) and sequenced.

Teratoma formation and generation of chimeric mouse

$1x10^6$ CiPSCs were subcutaneously injected into NOD-SCID mouse and teratoma formed from 4 to 8 weeks. For generation of chimeras, CiPSCs were injected into ICR blastocysts and transplanted into pseudopregnant ICR females. The resulting chimeric mice were determined for germline transmission by mating F2 mice with ICR mice. All of the animal experiments were performed with the approval and according to the guidelines of the Animal Care and Use Committee of the Guangzhou Institutes of Biomedicine and Health.

XEN chimera assay

For chimera test, mCherry-labeled XEN-like colonies were picked and disaggregated to a single cell suspension in 0.25% trypsin-EDTA. After trypsin neutralization, cells were centrifuge at 250 g for 5 min at room temperature and resuspended in M2 medium on ice bath. Approximately, 10 to 15 XEN-like cells, primary XEN cells or MEFs were injected into each blastocyst and transferred to the uterus of E2.5 pseudopregnant females. Chimera conceptus between E6.5-8.5 were dissected carefully to keep the parietal yolk sac intact and observed with fluorescence microscopy.

For the chimera test of MEFs, primary XENs or MEF derived XEN-like cells by our protocol (day 22) and Deng's protocol (day 12), cells were infected with pRLentiviral vectors possessing mCherry coding sequence for labeling.

ATAC-seq

ATAC-seq was performed as previously described (Buenrostro et al., 2013; Buenrostro et al., 2015). In brief, a total of 50,000 cells were washed once with 50 μL cold PBS and re-suspended in 50 μL lysis buffer (10 mM Tris-HCl pH 7.4, 10 mM NaCl, 3 mM $MgCl_2$, 0.2% (v/v) IGEPAL CA-630). The suspension was then centrifuged at 500 g for 10 min at 4°C, following by addition of 50 μL transposition reaction mix of Nextera DNA library Preparation Kit (96 samples) (FC-121-1031, Illumina). Then the samples were amplified by PCR and incubated at 37°C for 30min. DNA was isolated using a MinElute Kit (QIAGEN). ATAC-seq libraries were subjected to 5 cycles for pre-amplification first, and then amplified by PCR for an appropriate number of cycles as described (Buenrostro et al., 2015). The amplified libraries were purified with a Qiaquick PCR (QIAGEN) column. The concentration of library was measured using a KAPA Library Quantification Kit (KK4824) according to the manufacturer's instructions. Library integrity was checked by gel electrophoresis. Finally, the ATAC library was sequenced on a NextSeq 500 using a NextSeq 500 High Output Kit v2 (150 cycles) (FC-404-2002, Illumina) according to the manufacturer's instructions.

ATAC-seq bioinformatics analysis and peaks calling

All the sequencing data were mapped onto the mm10 mouse genome assembly using the bowtie2 software. Low quality mapped reads were removed using samtools (view –q 35) and only unique reads mapping to a single genomic location or strand were kept. We removed mitochondrial sequences using 'grep –v 'chrM'. Biological replicates were merged, and peaks were called using dfilter (Kumar et al., 2013) (with the settings: -bs = 100 –ks = 60 –refine). BigWig files were produced by genome Coverage Bed from bedtools (scale = 107/ < each_sample's_total_unique_reads >) and then bed graph to BigWig. Gene ontology and gene expression measures were first called by collecting all transcription start sites within 10 kb of an ATAC-seq peak, and then performing GO analysis with goseq (Young et al., 2010). Other analysis was performed using glbase (Hutchins et al., 2014).

Transcription factor motif discovery and gene ontology

Motif analysis was performed using HOMER (Heinz et al., 2010) with default settings. Motifs were only kept when the P value was < 0.01 and (< percent of target > / < percent of background >) was > 1.5. Gene ontology enrichment was performed using goseq (Young et al., 2010), with default settings.

QUANTIFICATION AND STATISTICAL ANALYSIS

Data are presented as mean ± s.d. or mean ± s.e.m. as indicated in the figure legends. Unpaired two-tailed Student's t test, were used to assess statistical significant. The P value was calculated with the Prism 6 software. A P value < 0.05 was considered as statistically significant, *p < 0.05, **p < 0.01, ***p < 0.001. No statistical method was used to predetermine the sample size. The experiments were not randomized. The investigators were not blinded to allocation during experiment and outcome assessment.

DATA AND SOFTWARE AVAILABILITY

The accession number for the ATAC-seq and RNA-seq data for OKS(YIP) induced reprogramming reported in this paper is GEO: GSE93029.

The accession number for the ATAC-seq, RNA-seq, and ChiP-Seq data for chemical induced reprogramming reported in this paper is GEO: GSE110264.